788 *Biochemistry* **2011,** *50,* 788–794
DOI: 10.1021/bi1019258

BIOCHEMISTRY
including biophysical chemistry & molecular biology
Article

Structure of a Slow CLC Cl^-/H^+ Antiporter from a Cyanobacterium†

Hariharan Jayaram, Janice L. Robertson, Fang Wu, Carole Williams, and Christopher Miller*

Department of Biochemistry, Howard Hughes Medical Institute, Brandeis University, Waltham, Massachusetts 02454, United States

Received December 2, 2010; Revised Manuscript Received December 21, 2010

ABSTRACT: X-ray crystal structures have been previously determined for three CLC-type transporter homologues, but the absolute unitary transport rate is known for only one of these. The *Escherichia coli* Cl^-/H^+ antiporter (EC) moves ~2000 Cl^- ions/s, an exceptionally high rate among membrane-transport proteins. It is not known whether such rapid turnover is characteristic of ClCs in general or if the *E. coli* homologue represents a functional outlier. Here, we characterize a CLC Cl^-/H^+ antiporter from the cyanobacterium *Synechocystis* sp. PCC6803 (SY) and determine its crystal structure at 3.2 Å resolution. The structure of SY is nearly identical to that of EC, with all residues involved in Cl^- binding and proton coupling structurally similar to their equivalents in EC. SY actively pumps protons into liposomes against a gradient and moves Cl^- at ~20 s^{-1}, 1% of the EC rate. Electrostatic calculations, used to identify residues contributing to ion binding energetics in SY and EC, highlight two residues flanking the external binding site that are destabilizing for Cl^- binding in SY and stabilizing in EC. Mutation of these two residues in SY to their counterparts in EC accelerates transport to ~150 s^{-1}, allowing measurement of Cl^-/H^+ stoichiometry of 2/1. SY thus shares a similar structure and a common transport mechanism to EC, but it is by comparison slow, a result that refutes the idea that the transport mechanism of CLCs leads to intrinsically high rates.

The CLC family of Cl^- transport proteins is made up of two mechanistically distinct subclasses: Cl^- channels and Cl^-/H^+ exchangers (also called antiporters). These proteins, which enable transmembrane movement of Cl^- (or, in plants, NO_3^-) for many different physiological purposes throughout the biological world, have been extensively investigated by electrophysiological, biochemical, and crystallographic techniques (*1*, *2*). Only CLC-ec1, a Cl^-/H^+ exchanger from *Escherichia coli*, has yielded to all three approaches. Accordingly, this homologue (henceforth denoted EC) has provided a unique paradigm for structure−function analysis of CLC proteins. Some of its basic properties, such as its homodimeric architecture, its anion binding and selectivity characteristics, and its 2-for-1 Cl^-/H^+ exchange stoichiometry, also appear in all known CLC exchangers. But other characteristics of EC do not apply generally to the CLC family; all eukaryotic and some prokaryotic CLC proteins, for example, carry a large cytoplasmic C-terminal regulatory domain (*3*) which is absent in EC and in many other bacterial homologues. A striking feature of EC is its absolute turnover rate, 2000−3000 s^{-1} (*4*, *5*), which is atypically high among all varieties of transporters. Moreover, this rate can be increased ~20-fold further by "channelizing" the protein's ion-binding region through designed mutagenesis (*6*). Since EC is the only CLC transporter for which this fundamental kinetic property has been determined, it is impossible to judge whether this high rate is intrinsic to CLC mechanisms or whether it is an outlier within this family.

For these reasons, we have been seeking additional CLC homologues appropriate for analysis of both structure and function. Here we report an X-ray crystal structure of CLC-sy1 (denoted SY herein), a cyanobacterial CLC of the exchange-transporter subclass. The structure of SY is very similar to that of EC, with which it shares 39% sequence identity (Figure 1), and its fundamental transport characteristics are conserved as well. But SY displays a transport rate about 100-fold lower than that of EC. By comparing EC and SY sequences, we locate two residues which, when mutated to the equivalent in EC, substantially increase the SY turnover rate, while supporting the 2-to-1 Cl^-/H^+ coupling stoichiometry typical of CLC exchangers. These results provide functional and structural information for an additional CLC exchanger, which enriches comparative studies of the mechanism of Cl^- and H^+ transport in this family of proteins.

MATERIALS AND METHODS

Special reagents were obtained from Avanti (lipids), Anatrace (detergents), and Roche (Lys-C protease). An open reading frame (gi 1652876) coding for a 451-residue CLC protein was cloned from the cyanobacterium *Synechocystis* sp. PCC6803. This sequence was inserted into the pASK vector with a C-terminal hexahistidine tag (*7*), as diagramed in Supporting Information Figure 1. Protein was expressed in *E. coli* with growth conditions described for EC (*8*). Cells were lysed by sonication and extracted in 40 mM decyl maltoside (DM)[1] for 1−2 h at room temperature. After the extract was clarified by centrifugation (25000*g*, 45 min), the supernatant was passed through cobalt-affinity beads (1 mL of resin/L of bacterial culture), washed with 100 mM NaCl, 20 mM imidazole, and eluted with 400 mM imidazole. The protein was further purified

†Supported in part by NIH Grant GM-31768.
*To whom correspondence should be addressed. E-mail: cmiller@brandeis.edu. Phone: 781-736-2340. Fax: 781-736-2365.

[1]Abbreviations: FCCP, carbonyl cyanide *p*-trifluoromethoxyphenylhydrazone; DM, *n*-decyl maltoside; PEG, polyethylene glycol.

 Published on Web 12/21/2010

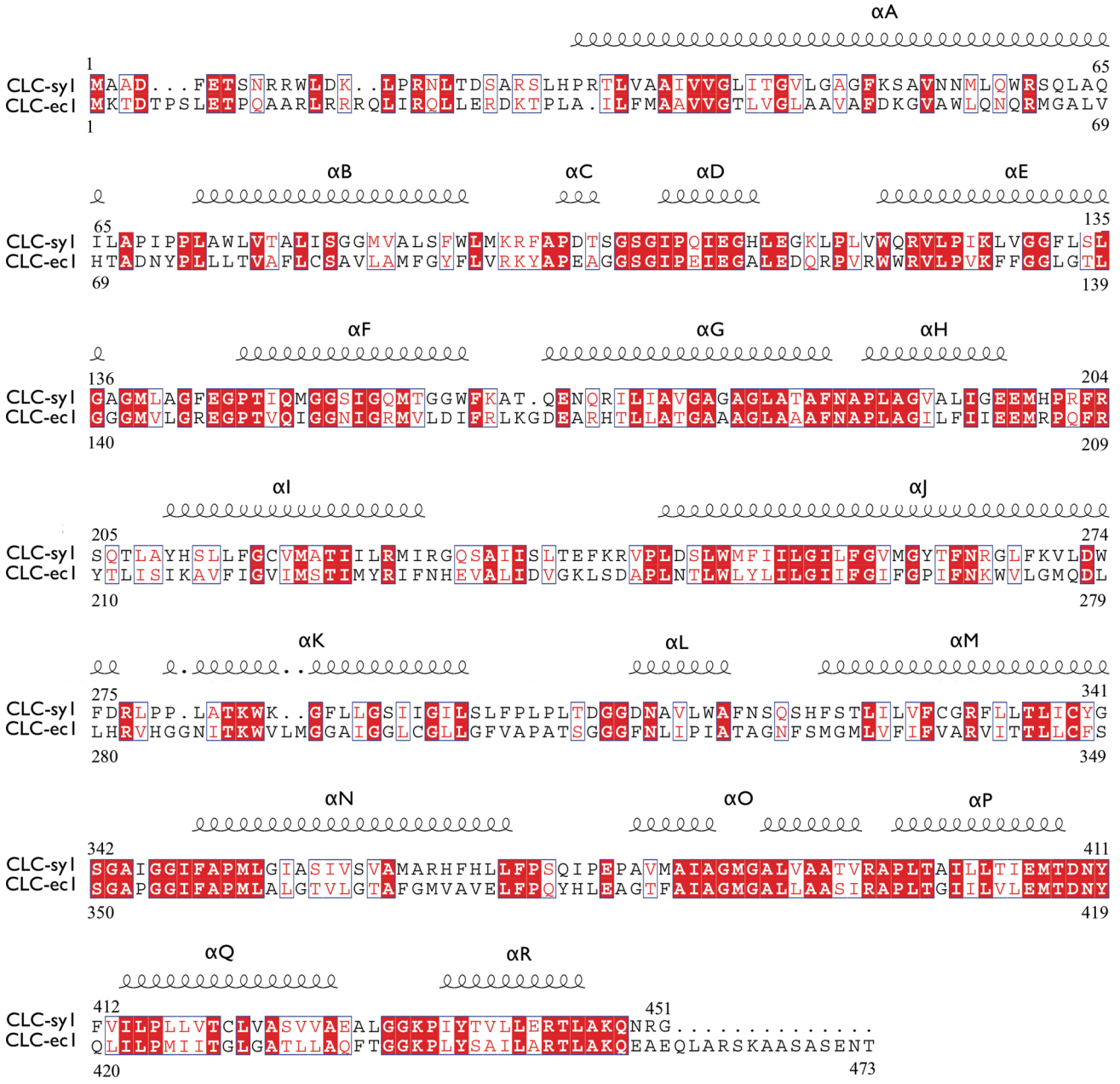

FIGURE 1: Alignment of CLC-sy1 and CLC-ec1 sequences. Solid red block represents identical residues, comprising 39% of the total sequence. The boxed segments highlight both identical and similar parts of the alignment. The 18 α-helices forming the transmembrane structure are labeled αA−αR.

on a Superdex 200 gel filtration column in 100 mM NaCl, 20 mM Tris-HCl, pH 7.5, and 5 mM DM. For crystallization experiments, the preparation was treated with lysine-C endoproteinase (1 h, 0.01 unit/mg, 25 °C) before the Superdex 200 step to remove the first 14 N-terminal residues. Crystals were grown by vapor diffusion for 3−12 days in sitting drops at 18−25 mg/mL protein with ~40 mM DM. The drops were set with 2 μL of protein mixed with 1−2 μL of reservoir solution containing 30−32% PEG 400, 200 mM $CaCl_2$, and 100 mM Tris-HCl, pH 8.0−8.2; additives were then introduced to the indicated final concentrations: C-Hega-11 (14 mM), $SrCl_2$ (12 mM), PEG 400 (6.2%), and in some cases Hega-10 (9 mM) and decanoyl sucrose (3 mM). Only crystals larger than ~200 μm diffracted well enough for data collection. The structure was solved by molecular replacement with PHASER using the EC homodimer (PDB 1OTS) as search model and prime-and-switch density modification to suppress model bias. The model was refined using Refmac5 and Phenix (*9*, *10*).

For functional analysis, purified SY protein was added to reconstitution buffer at 5−10 μg of protein/mg of lipid containing 20 mg/mL *E. coli* polar lipid and 35 mM CHAPS. Detergent was removed by dialysis against the desired intraliposomal solution over 36 h. For concentrative uptake experiments, liposome samples (100 μL) containing 450 mM KCl and 25 mM citrate−phosphate, pH 7.0, were centrifuged through 1.5 mL G50 columns equilibrated in uptake buffer (400 mM sorbitol, 25 mM citrate-phosphate, pH 4.0−7.0). $^{36}Cl^-$ (1 mM) was added to the extraliposomal solution to start the uptake, and liposomes were collected at various time points by passage through a 1.5 mL Dowex 1-X4 glutamate column (*7*). Proton pumping experiments were carried out with 300 mM KCl and 40 mM citrate, pH 4.8, for the internal solution; liposomes were spun through Sephadex G50

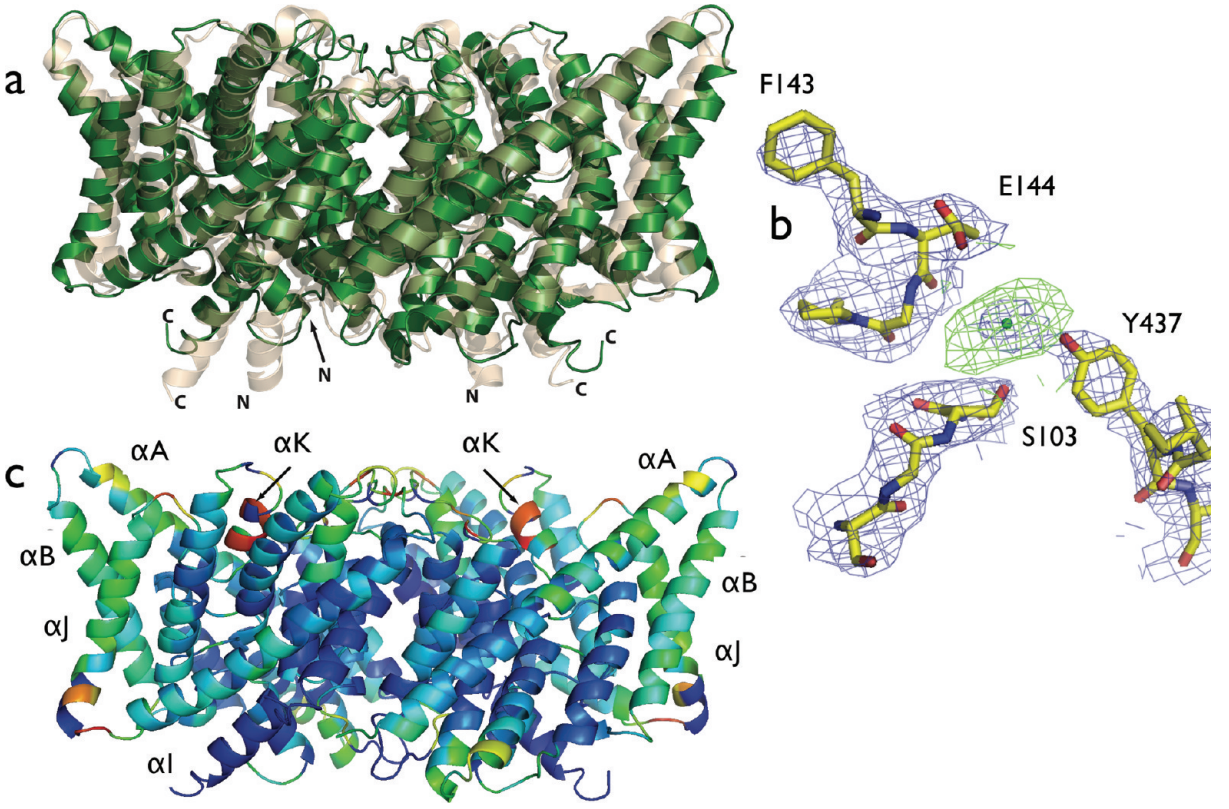

FIGURE 2: Structure of SY. (a) SY (green) and EC (tan) structure alignment of backbone atoms (1.3 Å rmsd). (b) The central Cl^- binding site in SY, formed by residues S103 and Y437. The external H^+-transfer residue, E144, and its adjacent residue, F143 are also shown, with $2F_o - F_c$ map (blue) and anomalous difference density from a Br^- data set (green) contoured at 1.5σ and 8σ, respectively. (c) Regions of structural agreement of SY and EC mapped onto SY structure. Low rmsd regions are shown in blue, while increasing values of rmsd are in green, yellow, and red. Helices αA, αB, αJ, and αK are labeled as shown. Structure factors and coordinates of SY are deposited in the PDB (3NCO for the Cl^- structure and 3Q17 for the Br^- structure).

columns equilibrated in external buffer (300 mM K^+-isethionate, 1 mM KCl, 2 mM citrate−KOH, pH 4.8) and then diluted 10-fold into a stirred cell containing 1.8 mL of this solution. Valinomycin (Vln, 0.5 μM) was added to set the membrane potential to zero and initiate transport. The resulting proton uptake was followed by recording external pH with a glass electrode, and after reaching a steady level the pH gradient was dissipated by addition of 0.5 μM proton ionophore FCCP. Initial rate of Cl^- efflux uncoupled from H^+ uptake (*4*) was measured under similar conditions, except that 25 mM citrate was included in internal and external solutions and efflux was started by addition of Vln and FCCP together; Cl^- appearance in the external solution was recorded electrochemically with a Ag/AgCl electrode. After several minutes, liposomes were disrupted by addition of 50 mM octyl β-glucoside to measure total trapped Cl^-. Cl^-/H^+ stoichiometry is reported as the ratio of initial rates (measured from the first 5 s of uptake) under proton-pumping conditions, with calibration by 150 nmol of HCl. For isothermal calorimetry (ITC) measurements, protein was purified as described above except that the final gel-filtration step was carried out in Cl^--free buffer: 100 mM Na^+/K^+ tartrate, 20 mM Na_2HPO_4, pH 7.5, and 5 mM DM. Protein was concentrated to 200 μM, and ITC was performed in a 1.8 mL cell using 5 μL injections of 10 mM NaCl in the gel-filtration buffer.

The refined SY model was used for electrostatic analysis. The static field contribution of each residue was calculated at the central Cl^- binding site by solution of the Poisson equation as described (*11*). As this computation was used merely for screening residue contributions, the calculations were carried out with the protein alone, without a membrane dielectric implementation. The protein dielectric constant was set to 4 and solvent to 80, and all residues were in native protonation states, with histidines set neutral. All calculations were carried out using the PBEQ module of CHARMM (*12*).

RESULTS

Crystal Structure of SY. Initial poorly diffracting, needle-like crystals appearing in PEG400 screens were improved by using three extra detergents and $SrCl_2$ as additives. Even with these optimized conditions, diffraction was typically anisotropic with high mosaicity, but a few rare crystals were suitable for structure determination at 3.2 Å resolution. The EC homodimer served as a molecular replacement search model, locating a single SY homodimer in the asymmetric unit (Supporting Information Figure 2). Model bias was suppressed by refinement using prime-and-switch density modification (*13*), which was particularly powerful because of the high solvent content (80%) of these crystals. The resulting electron density maps allowed unambiguous tracing of the entire transmembrane region, residues 26−450 (crystallographic statistics reported in Supporting Information Table 1).

The SY structure (Figure 2a) closely matches that of its *E. coli* homologue (C_α rmsd 1.3 Å). The protein is a homodimer in which each subunit, constructed from 18 α-helices, is mostly membrane-embedded. The transmembrane dimer interface (~1200 $Å^2$) in SY is composed mainly of interdigitating alkyl side chains projecting off helices αH, αI, αP, and αQ, as in EC (*14*). The key ion-coupling residues of EC all overlay their

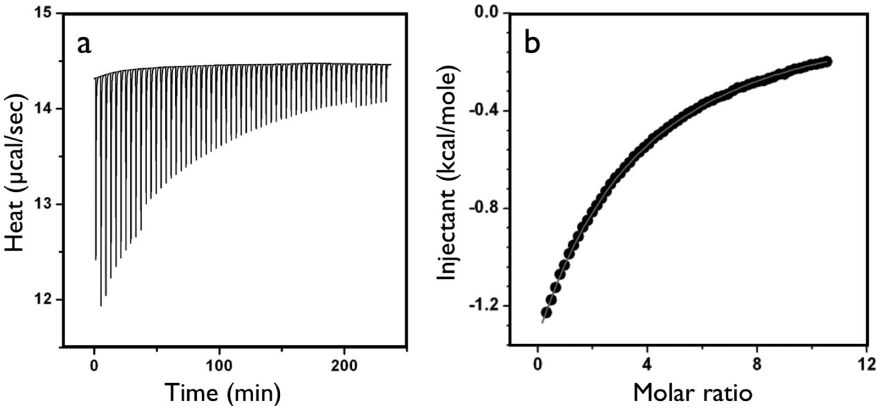

FIGURE 3: Equilibrium binding of Cl^- to SY. (a) Traces of heat evolution in ITC run. SY at 216 μM in DM micellar solution was challenged with NaCl injections. (b) Binding isotherm. Integrated heats (filled points) were fit to single-site Cl^- binding isotherm (solid curve), with K_D = 1.5 mM. Thermodynamic parameters for binding are $\Delta H^\circ = -10$ kcal/mol and $\Delta S^\circ = -21$ cal/(mol K). A duplicate experiment gave essentially identical results.

equivalents in the SY structure (Figure 2b): the external and internal proton-transfer glutamates (E144 and E198, respectively) and the central serine−tyrosine pair (S103−Y437), which forms the intracellular gate or kinetic barrier of the Cl^- pathway (*3*, *6*). The central Cl^- ion is visible in Fourier difference maps, as is confirmed in anomalous difference maps from crystals grown in Br^-. As in EC, this buried, dehydrated anion is coordinated by the central Ser and Tyr side chains, as well as by several backbone amides.

The SY structure shows a few minor departures from that of EC. The backbone trajectories of outer helices αA-αC, αJ, and αK are slightly displaced from those in the molecular replacement model (Figure 2c), but no significant changes in regions known to mediate Cl^-/H^+ transport arise from these differences. In addition, the bound central Cl^- ion density in SY is less prominent than in EC (*15*, *16*). Equilibrium Cl^- binding to SY, determined by ITC (Figure 3), yields K_D ~1.4 mM, about 2-fold higher than the value previously reported for EC (*5*); since crystals were grown at Cl^- concentrations far higher than this, we assign the weaker Cl^- density to the poorer quality of SY vs EC crystals, rather than to lower ion occupancy. Another difference in the SY structure is the absence of a second Cl^- ion, the weakly bound "internal" Cl^- seen in EC at the intracellular end of the Cl^- pathway (*15*−*17*), as is corroborated by our failure to observe anomalous difference density in this region with crystals grown in Br^-. In contrast to the mechanistically pivotal central Cl^-, the internal Cl^- ion is thought not to participate directly in transport (*5*, *18*), and so its absence here is not alarming.

Functional Characteristics of SY. The structural similarities above suggest that SY will hold few functional surprises. Indeed, this is the case. The protein's transport characteristics were assessed by reconstitution into liposomes. As with EC (*8*), SY supports acid-activated Cl^- flux (Figure 4a), with a somewhat stronger pH dependence than for EC (*8*). As with EC, competition of $^{36}Cl^-$ uptake by nonradioactive anions (Figure 4b) reveals little selectivity among Cl^-, Br^-, and NO_3^-, while SCN^- competes strongly and SO_4^{2+} weakly, the divalent anion requiring 10-fold higher concentration for effects comparable to Cl^-. The central mechanistic feature of CLC exchangers, Cl^-/H^+ antiport, is also observed in SY, as shown by uphill H^+ pumping at the expense of an oppositely directed Cl^- gradient (Figure 5). Here, liposomes are loaded with high Cl^- (300 mM) and suspended in low Cl^- (1 mM), with internal pH slightly lower than external. Upon addition of Vln to counteract the charge

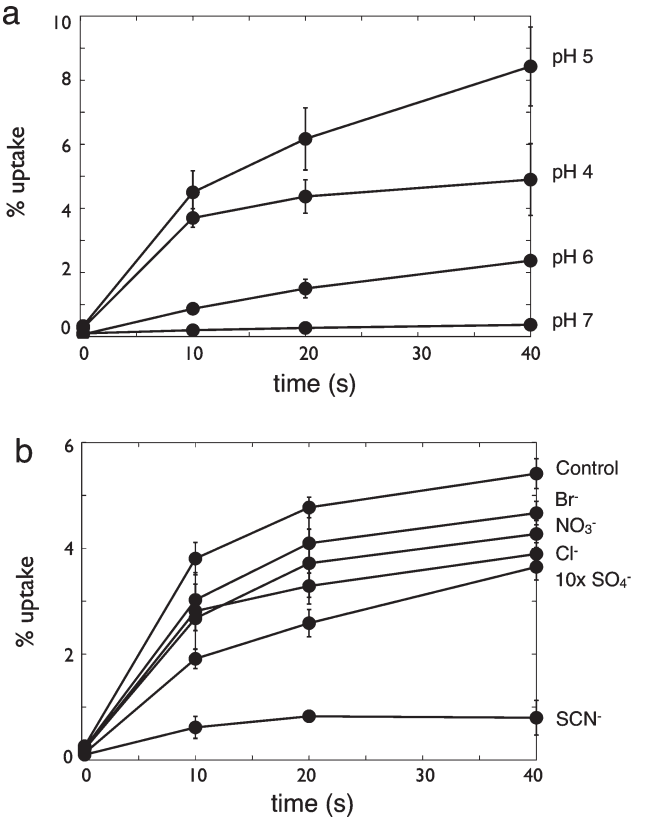

FIGURE 4: $^{36}Cl^-$ transport by SY. (a) Acid-activated concentrative uptake. Proteoliposomes were preequilibrated, and $^{36}Cl^-$ uptake time courses were performed at the indicated pH values. Uptake is reported as % of total $^{36}Cl^-$ counts that become trapped inside the liposomes. (b) Anion selectivity of transport. Selectivity was measured by inhibition of $^{36}Cl^-$ uptake by addition of nonradioactive anions (1 mM for monovalent anions and 10 mM for SO_4^{2-}). The control curve represents no addition of competing anions. Measurements were carried out at pH 4.5.

imbalance set up by electrogenic Cl^-/H^+ exchange, the suspension alkalinizes as H^+ is pumped inward, an effect reversed by a proton ionophore. While these ion movements qualitatively mimic those in EC, SY gives much smaller signals in our assays. We therefore suspected that the absolute turnover rate of SY might be much lower than the high value to which EC has accustomed us (*4*). This expectation is confirmed in a "Cl^- dump" experiment (*4*), wherein Cl^--loaded liposomes passively

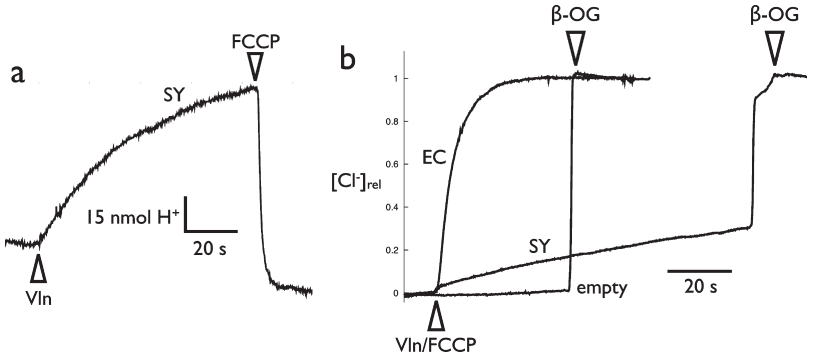

FIGURE 5: H^+ and Cl^- transport by SY. (a) H^+ pumping driven by a Cl^- gradient. Raw recordings of external solution pH are shown following addition of Vln at arrow to Cl^--loaded liposomes to start the Cl^-−H^+ exchange; upward deflection represents alkanization. Proton buildup was dissipated at end of the uptake by addition of proton ionophore FCCP as indicated. (b) Passive Cl^- efflux. Recordings of Cl^- appearance under similar conditions, except that FCCP was present throughout to prevent buildup of H^+ gradient. Liposomes were disrupted with 50 mM octyl β-glucoside (β-OG) to determine total trapped Cl^- which was used for normalization in calculating relative Cl^-. Efflux traces are indicated for EC, SY, and protein-free liposomes.

Table 1: Cl^- Turnover Rate for SY and Specific Mutants[a]

mutant	unitary Cl^- rate (s^{-1} per subunit)	mutant	unitary Cl^- rate (s^{-1} per subunit)
protein free	4 ± 2	E238K	15 ± 6
WT	20 ± 3	D309F	105 ± 7
K50D	14 ± 1	E429Q	14 ± 2
Q107E	26 ± 7	F143R/D309F	149 ± 21
F143R	130 ± 5	K50D/F143R/D309F	84 ± 14
F143K	14 ± 1	E144A/T437A	19 ± 2
F143H	22 ± 3		

[a]Cl^- turnover rates were measured electrochemically as in Figure 5b for the indicated SY variants (and control protein-free liposomes). Each value represents mean ± SE of three to four separate determinations (or range of duplicates for F143R/D309F).

release their contents into low-Cl− medium with no pH gradient present. The unitary turnover rate of SY is 20 s^{-1} (Table 1), a conventional value for transporters but 100-fold lower than the EC rate. This low turnover rate made it impossible to quantify the Cl^-/H^+ exchange stoichiometry for wild-type SY or to obtain satisfactory electrical recordings of SY in planar lipid bilayers, as is routinely accomplished with EC (*8*, *19*).

To seek residues responsible for the slow transport rate in SY, we carried out a comparative analysis of SY and EC sequences informed by their crystal structures. In particular, we focused on residues differing between SY and EC in electrostatics in the transport pathway, a factor that may account for the slightly weaker Cl^- binding affinity for SY. The static field contribution of each residue in the protein was evaluated at the central Cl^- binding site by solution of the continuum electrostatic Poisson equation. A residue-by-residue comparison of the two proteins shows several positions potentially capable of modulating the electrostatics along the transport pathway (Figure 6). Mutations at these positions to the corresponding EC residues are expected to be stabilizing (F143R, H200K, H211R, E238K, D309F, E429Q) or destabilizing (K50D, Q107E) for Cl^-. Most of these residues are located near the water-exposed surfaces and are thus likely to exert relatively weak effects. However, three residues, K50, F143, and D309, are partly buried and close to the Cl^- binding pathway. Residues F143 and D309 cap the N-termini of the αF and αL helices, respectively, which point their positive dipoles toward the external Cl^- binding site, and F143 is also adjacent, in sequence and structure, to the external glutamate gate E144. Furthermore, analysis of 2625 CLC homologues in the PFAM database shows that either Arg or Lys is found at the F143 equivalent position in over 70% of the entries, with zero occurrence of negatively charged residues (Supporting Information Table 2). Remarkably, Phe appears at this position only once, in the entry for SY. Position 309 is more evenly distributed among residue types, showing a significant preference for Tyr.

Each of the eight single substitutions listed above was reconstituted into liposomes, and unitary Cl^- transport rates were measured by the "Cl^- dump" assay (Figure 7a). The rates are similar to wild-type SY for most constructs (Table 1), except for the two external site mutants F143R and D309F, each of which showed an ~5-fold increase in Cl^- transport to 130 and 105 s^{-1}, respectively. The increase in rate accompanying these mutations made it possible to measure the Cl^-/H^+ transport stoichiometry. The F143R mutant (Figure 7b) maintains H^+ pumping, with Cl^-/H^+ exchange stoichiometry close to the 2:1 value as expected for CLC transporters (*2*), further corroborating the mechanistic similarity between SY and EC. We also examined the double substitution, F143R/D309F, which further increased the rate only slightly to ~150 s^{-1} (Figure 7a). We noticed the possibility of a functional triad formed by these two residues and K50 (Figure 6), since these three sites in EC (Asp + Arg + Phe) and SY (Lys + Phe + Asp) conserve charge. However, the SY triple mutant (K50D, F143R, D309F), which recapitulates the EC triplet, fails to produce a fast transporter (85 s^{-1}). At first glance, it appears that Cl^- transport rates in SY correlate with net charge of this external region, but this conclusion is undermined by further experiments. For instance, in contrast to F143R, Lys or His substitutions here have no effect on transport (Table 1). Likewise, the converse mutation in EC, R147F, shows only a modest (~30%) lowering of transport rate. For these reasons, we cannot invoke a general electrostatic mechanism to account for the large differences in SY and EC rates. There is a certain irony

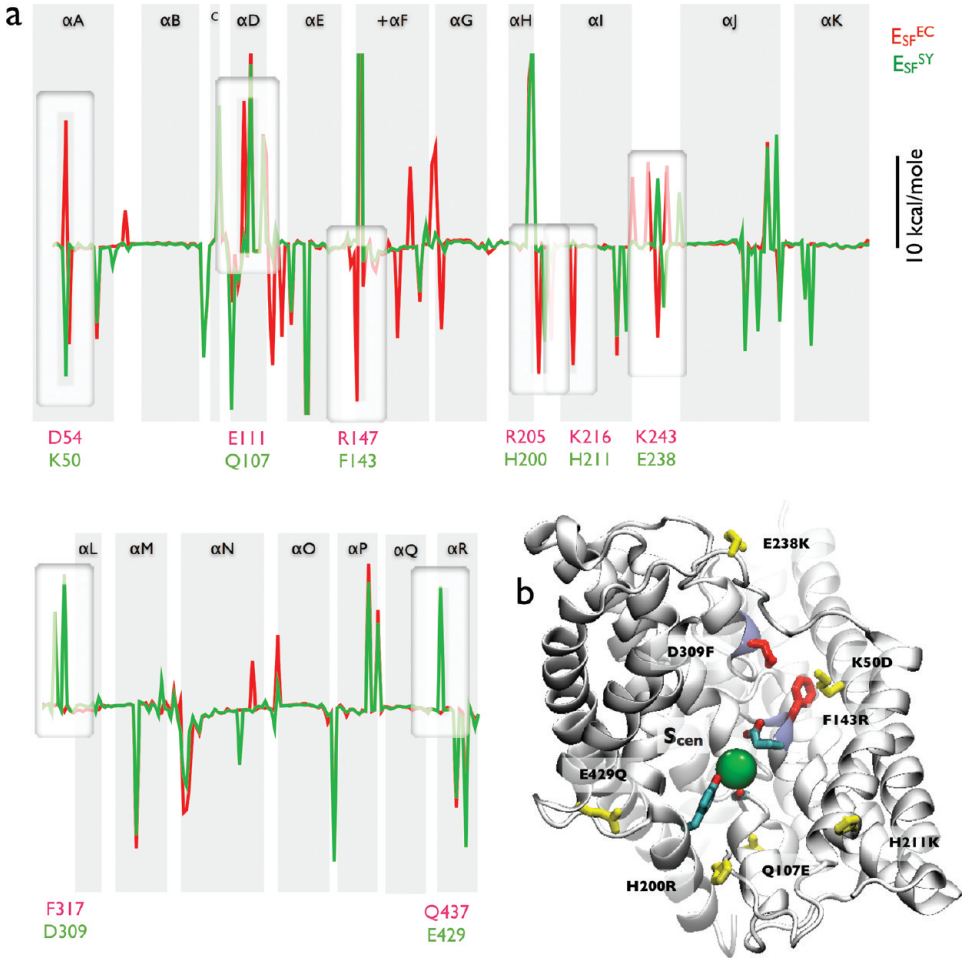

FIGURE 6: Electrostatic analysis of residues affecting Cl^- binding in SY and EC. (a) Static field contribution for each residue in SY (green) and EC (red) for a Cl^- ion bound to the central site. Deflections represent stabilizing (downward) or destabilizing (upward) energies for Cl^- binding. Residues showing significant differences between SY and EC are highlighted. (b) Single subunit of SY viewed from the dimer interface, with helices H, I, P, and Q removed for visualization of the Cl^- binding pathway. Residues near the central site (Y437, S103) and the external gate (E144) are shown. Residues with significant differences in electrostatics between SY and EC are highlighted in yellow, and the two residues (F143, D309) adjacent to the external site (blue ends of helices) are highlighted in red.

in this conclusion since F143 and D309 were originally identified as influential via an electrostatic computation.

In a final, desperate attempt to increase the transport rate of SY, we resorted to radical surgery by removing both external and internal "gates" of the transporter's Cl^- pathway. In EC, removal of these gates by the double mutation E148A/Y445A produces a continuous pore connecting internal and external solutions, abolishes H^+ transport, and increases Cl^- transport to ~20000 s^{-1} (*6*). Since the structure of SY is so similar to EC, we expect that removal of the gates should also greatly speed transport. However, the corresponding mutation in SY, E144A/Y437A, produces no change whatsoever over the slow Cl^- transport rate of wild-type SY (Figure 7A). This result is extremely surprising, but without a crystal structure of the double mutant, which we have still not achieved, we cannot fathom its meaning.

DISCUSSION

Until now, X-ray crystal structures of three CLC Cl^-/H^+ exchange transporters have been determined: of prokaryotic homologues from *E. coli* and *Salmonella enterica typhimurium* (*17*, *20*) and of a eukaryotic CLC from *Cyanidioschyzon merolae* (*3*). Of these, only EC has been subjected to detailed analysis of transport function, including quantitative measurements of the unitary turnover rate (*4*, *5*). Moving Cl^- ions at 2000−3000 s^{-1} at 25 °C, EC is an unusually fast transporter. In light of the unusual structural architecture of CLC proteins and the absence of large conformational changes during the transport cycle, which appears to involve only subtle side chain rearrangements (*3*, *18*, *21*), we have naturally suspected that atypically high transport rates may be a feature of all CLC transporters. This suspicion is buttressed by the similarities between SY and EC. All key structural elements, the transmembrane helices, Cl^- binding residues and gates, and residues involved in H^+ transport, are found similarly disposed in the two homologues, and the mechanistic hallmark of CLC transporters, 2:1 Cl^-/H^+ antiport stoichiometry, is also present in SY.

But our results refute this expectation without ambiguity. At 20 s^{-1}, Cl^- transport in SY is 2 orders of magnitude slower than in EC, with a rate conventional for membrane transporter mechanisms. This striking difference in rate between the two homologues must lie in subtle structural variation and sequence differences. We have identified two residues in SY that increase the transport rate when mutated to their EC counterparts, F143R and D309F, substitutions that increase the local positive electrostatic character of the protein's ion-transport region. Positioned at the N-terminal ends of the two helices pointed at the external Cl^- site and adjacent to the external glutamate gate, these

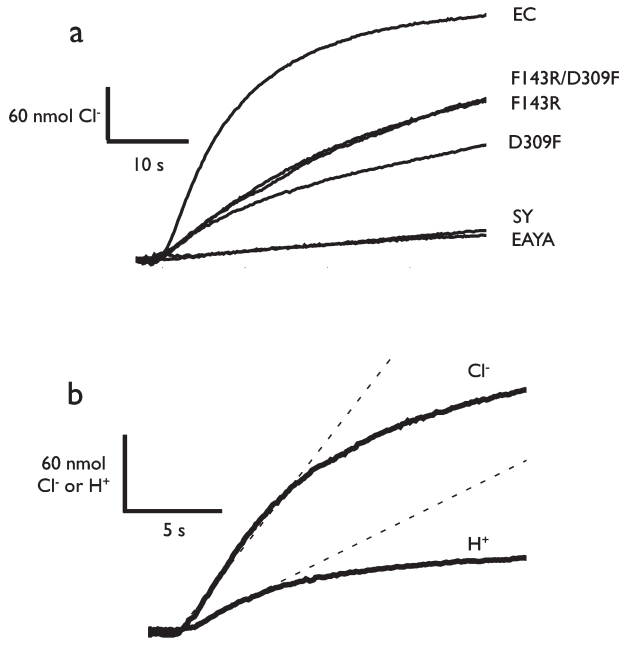

FIGURE 7: SY turnover rates and antiport stoichiometry. (a) Passive Cl^- efflux. Raw recordings of Cl^- release are shown for SY and indicated mutants, and rates are reported in Table 1. Protein was reconstituted at 5 μg of protein/mg of lipid, except E144A/Y437A (EAYA) which was at 10 μg/mg. (b) Stoichiometry of Cl^-/H^+ transport in F143R mutant. Stoichiometry is measured by comparing initial rates of transport (dashed lines); Cl^-/H^+ stoichiometry was determined to be 2.3 ± 0.4 (SE, $N = 3$). Cl^- and H^+ signals were calibrated by addition of 150 nmol of HCl.

residues appear to be in position to stabilize anions in the transport region. However, these mutations enhance transport only modestly, the double mutant F143R/D309F reaching only 8% of the EC rate. Nevertheless, SY now provides a structural model for comparison and a target for dissecting out new molecular contributors to transport function.

ACKNOWLEDGMENT

We are grateful to D. Kern for use of the ITC instrument and to R. Sah for advice on the manuscript.

SUPPORTING INFORMATION AVAILABLE

Figures and tables as described in the text. This material is available free of charge via the Internet at http://pubs.acs.org.

REFERENCES

1. Jentsch, T. J. (2008) CLC chloride channels and transporters: from genes to protein structure, pathology and physiology. *Crit. Rev. Biochem. Mol. Biol. 43*, 3–36.
2. Accardi, A., and Picollo, A. (2010) CLC channels and transporters: proteins with borderline personalities. *Biochim. Biophys. Acta 1798*, 1457–1464.
3. Feng, L., Campbell, E. B., Hsiung, Y., and MacKinnon, R. (2010) Structure of a eukaryotic CLC transporter defines an intermediate state in the transport cycle. *Science 330*, 635–641.
4. Walden, M., Accardi, A., Wu, F., Xu, C., Williams, C., and Miller, C. (2007) Uncoupling and turnover in a Cl^-/H^+ exchange transporter. *J. Gen. Physiol. 129*, 317–329.
5. Picollo, A., Malvezzi, M., Houtman, J. C., and Accardi, A. (2009) Basis of substrate binding and conservation of selectivity in the CLC family of channels and transporters. *Nat. Struct. Mol. Biol. 16*, 1294–1301.
6. Jayaram, H., Accardi, A., Wu, F., Williams, C., and Miller, C. (2008) Ion permeation through a Cl^--selective channel designed from a CLC Cl^-/H^+ exchanger. *Proc. Natl. Acad. Sci. U.S.A. 105*, 11194–11199.
7. Maduke, M., Pheasant, D. J., and Miller, C. (1999) High-level expression, functional reconstitution, and quaternary structure of a prokaryotic ClC-type chloride channel. *J. Gen. Physiol. 114*, 713–722.
8. Accardi, A., Kolmakova-Partensky, L., Williams, C., and Miller, C. (2004) Ionic currents mediated by a prokaryotic homologue of CLC Cl^- channels. *J. Gen. Physiol. 123*, 109–119.
9. Winn, M. D., Murshudov, G. N., and Papiz, M. Z. (2003) Macromolecular TLS refinement in REFMAC at moderate resolutions. *Methods Enzymol. 374*, 300–321.
10. Adams, P. D., Afonine, P. V., Bunkoczi, G., Chen, V. B., Davis, I. W., Echols, N., Headd, J. J., Hung, L. W., Kapral, G. J., Grosse-Kunstleve, R. W., McCoy, A. J., Moriarty, N. W., Oeffner, R., Read, R. J., Richardson, D. C., Richardson, J. S., Terwilliger, T. C., and Zwart, P. H. (2010) PHENIX: a comprehensive Python-based system for macromolecular structure solution. *Acta Crystallogr., Sect. D: Biol. Crystallogr. 66*, 213–221.
11. Robertson, J. L., Palmer, L. G., and Roux, B. (2008) Long-pore electrostatics in inward-rectifier potassium channels. *J. Gen. Physiol. 132*, 613–632.
12. Jo, S., Vargyas, M., Vasko-Szedlar, J., Roux, B., and Im, W. (2008) PBEQ-Solver for online visualization of electrostatic potential of biomolecules. *Nucleic Acids Res. 36*, W270–275.
13. Terwilliger, T. C. (2004) Using prime-and-switch phasing to reduce model bias in molecular replacement. *Acta Crystallogr., Sect. D: Biol. Crystallogr. 60*, 2144–2149.
14. Robertson, J. L., Kolmakova-Partensky, L., and Miller, C. (2010) Design, function and structure of a monomeric ClC transporter, *Nature 468*, 844−847.
15. Lobet, S., and Dutzler, R. (2005) Ion binding properties of the CLC chloride selectivity filter. *EMBO J. 25*, 24–33.
16. Accardi, A., Lobet, S., Williams, C., Miller, C., and Dutzler, R. (2006) Synergism between halide binding and proton transport in a CLC-type exchanger. *J. Mol. Biol. 362*, 691–699.
17. Dutzler, R., Campbell, E. B., and MacKinnon, R. (2003) Gating the selectivity filter in ClC chloride channels. *Science 300*, 108–112.
18. Nguitragool, W., and Miller, C. (2007) CLC Cl^-/H^+ transporters constrained by covalent cross-linking. *Proc. Natl. Acad. Sci. U.S.A. 104*, 20659–20665.
19. Accardi, A., and Miller, C. (2004) Secondary active transport mediated by a prokaryotic homologue of ClC Cl^- channels. *Nature 427*, 803–807.
20. Dutzler, R., Campbell, E. B., Cadene, M., Chait, B. T., and MacKinnon, R. (2002) X-ray structure of a ClC chloride channel at 3.0 Å reveals the molecular basis of anion selectivity. *Nature 415*, 287–294.
21. Miller, C., and Nguitragool, W. (2008) A provisional transport mechanism for a CLC-type Cl^-/H^+ exchanger. *Philos. Trans. R. Soc. London, Ser. B 364*, 175–180.